Biomaterials 181 (2018) 113–125

Contents lists available at ScienceDirect

Biomaterials

journal homepage: www.elsevier.com/locate/biomaterials

Dual drug delivery and sequential release by amphiphilic Janus nanoparticles for liver cancer theranostics

Lingyu Zhang[a], Manjie Zhang[a], Li Zhou[b], Qinghe Han[c], Xiangjun Chen[a], Shengnan Li[a], Lu Li[a,**], Zhongmin Su[a], Chungang Wang[a,*]

[a] Department of Chemistry, Northeast Normal University 5268 Renmin Street, Changchun, Jilin, 130024, PR China
[b] Department of Chemistry, École normale supérieure, UPMC Univ. Paris 06, CNRS, PSL Research University, 75005, Paris, France
[c] Radiology the Second Hospital of Jilin University, Changchun, Jilin, 130022, PR China

ARTICLE INFO

Keywords:
Amphiphilic Janus nanoparticles
Dual drug delivery
Optional sequential release
Bimodal imaging
Synergistic therapy

ABSTRACT

Co-delivery of two drugs with diverse physicochemical properties and specific administration order for cancer theranostics are vitally important for drug resistance conquering and side effects reducing. Consequently, we explored a unique amphiphilic PCL-AuNC/$Fe(OH)_3$-PAA Janus nanoparticle (JNP) to simultaneously preserve the hydrophilic drug (doxorubicin) and hydrophobic drug (docetaxel) in their distinct domains. Owing to their extraordinary heterostructure and independent pH and NIR sensitive properties, the optional sequential drug release by a single inorganic JNP was realized for the first time, and the results presented the synchronous release of two drugs had 5% better therapeutic effect. In addition, the excellent computed X-ray tomography/magnetic resonance (CT/MR) imaging capabilities from AuNC and $Fe(OH)_3$ suggested our JNPs could effectively guide the cancer therapy. Furthermore, the mice treated with dual drug loaded PCL-AuNC/$Fe(OH)_3$-PAA JNPs under near infrared (NIR) laser irradiation showed better tumor inhibition than solo drug, cocktail and dual drug treated groups, indicating the effectivity and significance of combined cancer therapy.

1. Introduction

Synergistic combination of two therapeutic agents or multimodal treatment strategies can conquer the severe drug resistance and prevent tumor relapse associated with traditional high dose of single drugs in treating cancers to achieve desirable therapeutic index [1–5]. Besides, administrating the drugs with different physicochemical properties and diverse mechanisms of drug action will get better therapeutic effect, especially in appropriate administrated sequence, which can induce quite different results, synergistic or even converse effect [6–11]. Up until recently, series of nanoplatforms, such as liposomes [12,13], dendrimers [14–16], polymeric nanoparticles (NPs) [17–19] and silica NPs [20–22] present the ability to co-encapsulate different drugs and delivery them to the diseased cells, thus eliminating the adverse side effects from cocktail administration of two free drugs. However, these carriers are almost with symmetrical geometry and simplex storage room, which can not meet the requirements including hosting drugs with diverse physiochemical properties (hydrophobic/hydrophilic), precise drug ratio and peculiarly releasing of drugs in an optimal sequence to reach the maximal therapeutic efficiency. Therefore, the major challenge in the field is not only to explore an efficient multidrug carrier with independent drug storage place and distinct polarity, but also to further schedule the release profiles.

Owing to the heterostructure, surface properties and various functionalities of inorganic Janus NP (JNP), they can host drugs with different solubility in their distinct domains without affect each other [23–27], facilitating the independent release of individual drugs compared to the conventional NPs normally with circumscribed drug release order. In addition, the two different segments can be designed to cooperate stimuli-responsive release properties (pH stimuli or NIR stimuli responsive capability) [28–30], cancer diagnosis (computed X-ray tomography (CT), fluorescence, magnetic resonance (MR) or photoacoustic (PA) imaging) [31–36], and multi-treatment (chemotherapy, photodynamic therapy (PDT) or photothermal therapy (PTT)) [37–43] together to enhance the treatment accuracy and efficiency. Although the inorganic JNPs show great application prospect in dual drug delivery, the relevant investigations are rarely reported. As we know, there is no report on designing a multifunctional dual drug delivery JNP, which combined the hydrophobic and hydrophilic drug delivery, CT/MR imaging and chemotherapy together with PTT *in vivo*, vitally

* Corresponding author.
** Corresponding author.
E-mail addresses: lil106@nenu.edu.cn (L. Li), wangcg925@nenu.edu.cn (C. Wang).

https://doi.org/10.1016/j.biomaterials.2018.07.060
Received 2 May 2018; Received in revised form 20 July 2018; Accepted 30 July 2018
Available online 30 July 2018

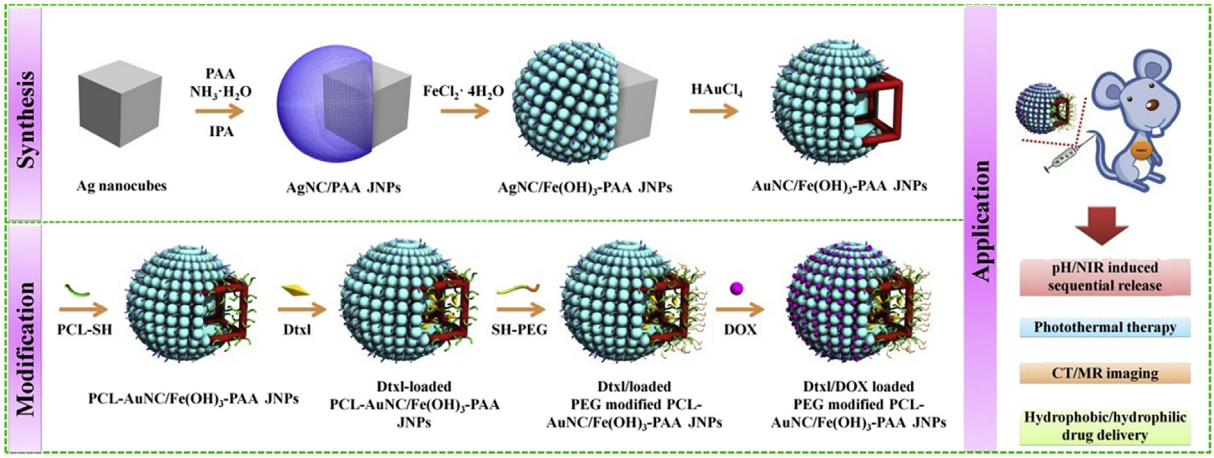

Scheme 1. Schematic illustration of the fabrication, modification and application of AuNC/$Fe(OH)_3$-PAA JNPs.

important, realized the optimal sequential therapy through pH/NIR controlled release.

Herein, we endeavor to design a novel amphiphilic poly(3-caprolactone)-gold nanocage/ferric hydroxide-poly(acrylic acid) (defined as PCL-AuNC/$Fe(OH)_3$-PAA) JNP for the first time with totally different morphologies, functionalities and surface properties in its two distinct sides, and further discuss their therapeutic effect of drug administrated order coupled with imaging-guided combined therapy. As shown in Scheme 1, the cubic-sphere like Ag/PAA JNPs were firstly prepared by mixing Ag nanocubes (AgNCs) with PAA, and used as the precursors. Then, the selective growth of $Fe(OH)_3$ on the PAA side endowed the Fe $(OH)_3$-PAA part with pH stimuli-responsive capability, MR imaging and hydrophilic drug loading properties. On the other side, the AgNC was etched by $HAuCl_4$ to form AuNC and then modified with PCL-SH, which made this part with NIR stimuli-responsive property, CT imaging and hydrophobic drug storage as well as PTT capability. Overall, our cage-sphere like PCL-AuNC/$Fe(OH)_3$-PAA JNPs with two independent parts were designed to combine the independent hydrophilic/hydrophobic drug delivery, NIR/pH stimuli-release property, CT/MR imaging, and photothermal effect in one unit for imaging-guided cancer theranostics, especially investigating the effect on sequential therapy.

2. Materials and methods

2.1. Materials

Ethylene glycol, $HAuCl_4{\cdot}3H_2O$, $AgNO_3$, doxorubicin hydrochloride (Dox), polyacrylic acid (PAA, $M_w \approx 1800$), tetraethyl orthosilicate (TEOS, ≥98%) and Poly(vinyl pyrrolidone) (PVP, Mw ~ 55,000) were bought from Sigma (USA). 3-Caprolactone (3-CL, 99%), bis(2-hydroxyethyl)disulfide (HES, 98%), Stannous octoate ($Sn(Oct.)_2$, 95%), dithiothreitol (DTT, 99%) and methoxy-poly(ethylene glycol)-thiol (SH-PEG, Mw ~ 5000) were purchased from energy chemical. Poly(vinyl pyrrolidone) (PVP, K-30) was from xilong scientific and $Na_2S{\cdot}9H_2O$ was from aladdin. Docetaxel (Dtxl) was purchased from San-bang. Ferrous chloride tetrahydrate ($FeCl_2{\cdot}4H_2O$), gadolinium(III) chloride hexahydrate ($GdCl_3{\cdot}6H_2O$), ethylene glycol (EG), ethanol, tetrahydrofuran (THF), isopropyl alcohol (IPA) and aqueous ammonia solution were purchased from Sinopharm Chemical Reagent Beijing Co., Ltd. Deionized (DI) water was used in all experiments.

2.2. Characterization

Transmission electron microscopy (TEM) was performed on a JEOL-2100F transmission electron microscope under 200 kV accelerating voltage. Fourier transform infrared spectroscopy (FTIR) was obtained on a Magna 560 FTIR spectrometer (Nicolet, USA). The X-ray photoelectron spectrum was carried out with an ECSALAB 250 using non-monochromatized Al Kα radiation. UV–Vis absorption spectroscopy was obtained on a U-3010 spectro-photometer (Hitachi, Japan). A CWdiode laser (LSR808H) with wavelength of 808 nm was used for the laser irradiation experiment. Inductively coupled plasma atomicemission spectroscopy (ICP-AES) was measured with Leeman ICP-AES Prodigy. 1H, 13C, and 19F NMR spectra were recorded on a 500 MHz or 600 MHz NMR spectrometer.

2.3. Synthesis of AgNC/PAA JNPs

Firstly, 6 mL ofEG was added into each of the four flasks at 150 °C for 2 h.Then, pipetting 70, 80, 90 and 100 μL of 3 mM Na_2S in EG solution into flasks. Waiting for 9 min, 1.5 mL of PVP (K-30) EG solution was added. Immediately thereafter, 0.5 mL of the $AgNO_3$ EG solution was added into each flask. The reaction was stopped when the reaction media appears green-ochre. Rinsing the silver nanocube (AgNC) twice with acetone and water, and finally dispersed in 10 mL water.

The obtained AgNC were mixed with PAA (80 μL, 0.2 mg mL^{-1}) under sonication for 10 min. Then, $NH_3{\cdot}H_2O$ (120 μL, 25–28%) was added with stirring for 10 min. After that, 40 mL of IPA were dripped into the flask to obtain the well-dispersed AgNC/PAA JNPs (water: IPA = 1: 4).

2.4. Synthesis of AgNC/$Fe(OH)_3$-PAA JNPs

With stirring, 600 μL of $FeCl_2{\cdot}4H_2O$ (10 mg mL^{-1}) was added in 3 portions into 50 mL AgNC/PAA JNPs solution. After 2 h, the AgNC/Fe $(OH)_3$-PAA JNPs were formed. Aging overnight, and then the product was centrifuged and washed with DI water, and re-dispersed in 4 mL water for next step.

2.5. Synthesis of AgNC/$Gd(OH)_3$-PAA JNPs and AgNC/SiO_2-PAA JNPs

The synthesis of AgNC/$Gd(OH)_3$-PAA JNPs is the same as AgNC/Fe $(OH)_3$-PAA JNPs except the addition of $GdCl_3{\cdot}6H_2O$ (10 mg mL^{-1}, 600 μL) instead of $FeCl_2{\cdot}4H_2O$.

To synthesize AgNC/SiO_2-PAA JNPs, 310 mL of IPA was added into the obtained 50 mL Ag/PAA JNPs. Then, 2.5 mL of $NH_3{\cdot}H_2O$ was added. After stirred for 30 min, the TEOS solution (3 mL, 20%) was added. After another 24 h, the product was washed with IPA and water.

2.6. Synthesis of AuNC/Fe(OH)$_3$-PAA, AuNC/Gd(OH)$_3$-PAA JNPs and AuNC/SiO$_2$-PAA JNPs

The AuNC/Fe(OH)$_3$-PAA JNPs was obtained though the galvanic replacement reaction. 100 mL of water and 1 g PVP (55,000) were mixed in a two-neck flask in 100 °C oil bath for 10 min. When the solution was boiling, 4 mL of as-prepared AgNC/Fe(OH)$_3$-PAA JNPs were added for another 10 min. Then, 1 mM $HAuCl_4$ solution was added slowly. UV–Vis spectrum was used to monitor the surface plasmon resonance (SPR) peak of the AuNCs, and the reaction was stopped until the SPR peak reached to near infrared (NIR) region. After refluxing for an additional 10 min until its color becomes stable and then cool the system to room temperature.

The synthesis of AuNC/Gd(OH)$_3$-PAA JNPs and AuNC/SiO$_2$-PAA JNPs is the same as the above protocol.

2.7. Surface modification

The PCL-SH was synthesis by ring-opening polymerization of 3-CL using HES as an initiator followed by reduction with tributyl phosphine. HES (154 mg), Sn(oct.)$_2$ (86 mg), 3-CL (8.6 g) and toluene (20 mL) was mixed in an oil bath at 100 °C for 24 h under an argon atmosphere. The reaction was terminated by adding excess HCl. The resulting polymer was precipitated in cold diethylether, filtrated and dried, and then dispersed in THF solution (20 mL). After that, tributyl phosphine (242 mg) was added and stirred at 25 °C for 24 h. The resulting polymer PCL-SH was precipitated in cold diethylether, filtrated under a N_2 flow, and dried.

The prepared PCL-SH (10 mg mL^{-1}, 500 μL) in THF was added into the AuNC/Fe(OH)$_3$-PAA JNPs solution. Allow the reaction to react for 4 h, the finally PCL-SH modified AuNC/Fe(OH)$_3$-PAA JNPs was harvested and re-dispersed in methanol.

2.8. Dual drug loading and releasing

The drug-loaded NPs were prepared by mixing Dtxl in methanol (10 mg mL^{-1}, 1 mL) with PCL-AuNC/Fe(OH)$_3$-PAA JNPs (1 mg) for 24 h. After centrifuged at 9000 rpm for 10 min and washed with water, 1 mg mL^{-1} SH-PEG was added and stirred for 2 h. After that, 1 mg mL^{-1} of Dox aqueous solution was added and re-dispersed, and then stirred for another 24 h. To evaluate the loading capacity of Dtxl and Dox, the contents of original Dtxl/Dox and residual Dtxl/Dox in supernatant were determined by UV–Vis measurements at 228 nm/480 nm. The loading capacity (LC) was calculated by Equation (1)

$$LC(\%) = \frac{m_{(initial)} - m_{(insupernatant)}}{m_{(initial)}} \times 100\% \quad (1)$$

To investigate the drug release property, the drug-loaded NPs were dispersed in 5 mL of PBS buffer (pH 7.4 and 5.3) with or without NIR irradiation (0.5, 0.7 and 1 W cm^{-2}, 5 min) at 37 °C, respectively. At selected time intervals, 200 μL of the samples was taken out and equal amount of fresh PBS was added. The amount of released Dox was measured by UV–Vis spectrophotometer (U-3010 spectro-photometer, Hitachi, Japan) and Dtxl was measured by high performance liquid chromatography (HPLC, Agilent 1200).

2.9. Photothermal heating effect

Different amount of PCL-AuNC/Fe(OH)$_3$-PAA JNPs (60, 30, 15 and 7.5 μg mL^{-1}, 1 mL) was suspended in centrifuge tube and exposed to an 808 nm laser (power density 1 W cm^{-2}, 5 min). The PCL-AuNC/Fe(OH)$_3$-PAA JNPs (15 μg mL^{-1}, 1 mL) was exposed to an 808 nm laser with different densities (0.5, 0.7, and 1 W cm^{-2}, 5 min). The temperature was recorded every 30 s and the images were acquired by a T460SC, infrared camera (FLIR, Sweden). DI water was also exposed to the NIR laser light as comparison group. Cyclic photothermal stability test was carried on by irradiating the solution of PCL-AuNC/Fe(OH)$_3$-PAA JNPs (15 μg mL^{-1}) for 5 min and waiting until the temperature recovered to room temperature, and then repeat for another 3 cycles. The photothermal conversion efficiency (η) was calculated by Equation (2) according to the previous reported method [44–46]

$$\eta = \frac{hS(T_{max} \quad T_{surr})Q_{dis}}{I(1 \quad 10^{A_{808}})} \quad (2)$$

h is the heat-transfer coefficient, S is the surface area of the container, T_{max} is the equilibrium temperature, T_{surr} is the ambient temperature of the surroundings, Q_{dis} expresses the heat associated with the light absorbance by the solvent, I is the incident laser power (1 W cm^{-2}), and A_{808} is the absorbance of the PCL-AuNC/Fe(OH)$_3$-PAA JNPs at 808 nm. The value of hS is derived according to Equation (3).

$$\tau_s = \frac{m_D C_D}{hS} \quad (3)$$

Where τ_s is the sample system time constant, m_D and C_D are the mass and heat capacity of water used as the solvent, respectively.

IR imaging of the whole H-22 bearing BALB/c mice treated with PBS and PCL-AuNC/Fe(OH)$_3$-PAA JNPs were carried out after exposing the tumors to the 808 nm laser (1.0 W cm^{-2}) for 5 min by using infrared cameras.

2.10. Cell culture

Human hepatocellular carcinoma (HepG-2) cells were grown as a monolayer in a humidified incubator in dulbecco's modified eagle medium (DMEM) supplemented with 10% fetal bovine serum at 37 °C in a 95% air 5% CO_2.

2.11. In vitro cytotoxicity study

The chemo-photothermal cytotoxicity of the samples was estimated by Cell Counting Kit-8 (CCK-8). HepG-2 cells were seeded into 96-well plates at a density of 5×10^4 cells per well and incubated for 24 h. The cytotoxicity of PCL-AuNC/Fe(OH)$_3$-PAA JNPs was checked by incubating the cells with our JNPs at different concentration for 48 h. The cell viability was measured by CCK-8 essay and calculated by Equation (4).

$$\text{Cell viability} = \frac{Abs_{(test\ cells)}}{Abs_{(control\ cells)}} \times 100\% \quad (4)$$

The sequential administration effect was implemented followed by a treatment schedule. Initially, the dual drug loaded JNPs (Dtxl/Dox/JNPs) were incubated with HepG-2 for 30 min, and then the medium was changed to fresh one. Within a period of 48 h, the cells were irradiated with NIR laser at lower density (0.5 W cm^{-2}, 5 min) at selected time point (0, 2, 6, 12, 24, 48 h). Under same condition, the pure JNPs were incubated with cells for 30 min, and then washed and further cultivated for another 48 h. The NIR only group is the cells treated with culture medium for 48 h, and then irradiated with NIR laser for 5 min. Finally, the cell viability was detected by CCK-8 essay.

To test the photo-chemotherapy, serum-free medium containing PBS, Dox loaded JNPs (Dox/JNPs), Dtxl loaded JNPs (Dtxl/JNPs), cocktail (Dox/JNPs and Dtxl/JNPs), and Dtxl and Dox co-loaded JNPs (Dtxl/Dox/JNPs) with various concentrations were added respectively to HepG-2 cells for 4 h. Then, the medium was removed and changed to fresh medium, and further cultivated for another 44 h to measure the cell viabilities. The photothermal effect was checked by incubating the PBS, JNPs, Dtxl/Dox/JNPs with and without NIR laser irradiation (1 W cm^{-2}, 5 min) at different concentrations with HepG-2 cells for 24 h, and the CCK-8 was added and incubated for another 2 h. The intensity was measured by using a plate reader (Tecan Infinite F200).

Combination index (CI) value is used to evaluate the synergistic effect of two drugs. IC_{50} is the drug concentration that inhibits a cellular

function or behavior by 50%, for each individual drug (A or B) or for the drug given as an A-B pair. If drug A and B act synergistically, CI is lower than 1. For drugs that act additively, CI is equal to 1. If CI is higher than 1, it acts antagonistically.

$$CI = \frac{IC_{50}(A)_{pair}}{IC_{50}(A)} + \frac{IC_{50}(B)_{pair}}{IC_{50}(B)} \quad (5)$$

2.12. Cell cycle and apoptotic

HepG-2 cells were treated with culture medium, JNPs, Dtxl/JNPs, Dox/JNPs, cocktail and Dtxl/Dox/JNPs with same drug concentrations (2 μg mL^{-1} Dox, 0.5 μg mL^{-1} Dtxl), respectively. After 48 h, the cells were harvest, washed and stained according to the protocol of Cell Cycle and Apoptosis Analysis Kit (Beyotime) and Annexin V-FITC Apoptosis Detection kit (Beyotime), respectively. The flow cytometry analysis was used to determine the cell cycle and apoptotic.

2.13. Hemolysis assay

Hemolysis test was carried out to evaluate the hematotoxicity of PCL-AuNC/Fe(OH)$_3$-PAA JNPs *in vitro* by using human red blood cells (RBCs, 2%), which was isolated by centrifugation and washing with 0.9% saline. Then, different concentrations of PCL-AuNC/Fe(OH)$_3$-PAA JNPs (15.625, 31.25, 62.5, 125, 250, 500 and 1000 μg mL^{-1}) was mixed with equal volume of RBCs suspension. PBS and water were used as negative and positive control. These samples were shaken and kept steady for 2 h at 37 °C. Finally, the mixtures were centrifuged at 3000 rpm for 3 min and the absorbance of the upper supernatants was measured by UV–Vis spectroscopy. The hemolysis percentage was calculated by Equation (6):

$$\text{Hemolysis}(\%) = \frac{A_{sample} - A_{control(-)}}{A_{sample(+)} - A_{control(-)}} \quad (6)$$

where A is the UV–Vis absorbance.

2.14. Fluorescence imaging

To verify the photothermal effect, HepG-2 cells were firstly seeded in a 96-well assay plate (2.5×10^4 cells per well). After 24 h, the cells were treated with PBS, PCL-AuNC/Fe(OH)$_3$-PAA JNPs (25 μg mL^{-1}), NIR only, and PCL-AuNC/Fe(OH)$_3$-PAA JNPs with NIR laser. After incubation for another 24 h, the cells were washed with PBS and exposed to NIR laser (808 nm, 1 W cm^{-2}) for 5 min. At this point, the IR thermal imaging of the culture plate was obtained. Then, the cells were stained with green calcein acetoxymethyl ester (calcein AM) and red propidium iodide (PI) for 10 min and imaged by a fluorescence microscope.

To test the combined chemo and photothermal effect, the seeded cells were treated with PBS, Dtxl/JNPs, Dox/JNPs, cocktail, Dtxl/Dox/JNPs with and without NIR laser. After 24 h, the cells were stained with green calcein AM and red PI for 10 min and imaged by a fluorescence microscope.

2.15. Biodistribution of PCL-AuNC/Fe(OH)$_3$-PAA JNPs in mice

The H-22 bearing BALB/c mice weighted about 15–18 g were intravenously injected with PCL-AuNC/Fe(OH)$_3$-PAA JNPs (25 mg kg^{-1}). The mice (n = 3) were then euthanized at different time points (6, 12, and 24 h), and the heart, liver, spleen, lung, kidney, and tumor were collected, weighed, and then treated with aqua regia at room temperature for several days to obtain clear solutions. The resulting solutions were diluted by DI water to 10 mL and subsequently analyzed by ICP-AES (Leeman ICP-AES Prodigy) to determine the total amount of Au in each measured organ.

2.16. In vitro and in vivo CT/MR imaging

For *in vitro* X-ray computed tomography/magnetic resonance (CT/MR) imaging, PCL-AuNC/Fe(OH)$_3$-PAA JNPs in 1 mL PBS with different concentrations were placed in a centrifuge tube. MR images were obtained by MesoMR23-060H-I. X-ray computed tomography (CT) images were obtained by using a SIEMENS SOMATOM Sensation 64 and the Hounsfield Unit (HU) variations were determined by using a syngo CT 2009S instrument (Siemens, Berlin).

For *in vivo* CT/MR imaging, 200 μL of the PCL-AuNC/Fe(OH)$_3$-PAA JNPs in PBS at the concentration of 5 mg mL^{-1} was injected via tail vein of H-22 bearing BALB/c mice. At selected time point (0 and 24 h), CT and MR images were obtained by using CT 2009S and discovery MR750 3.0T, respectively.

2.17. Combination therapy in vivo

The H-22 bearing BALB/c mice were randomly divided into 12 groups (n = 5 per group). Mice were injected intravenously by tail vein with 200 μL of different medium in PBS every two days. The amount of Dox, Dtxl and JNPs was 1.25, 0.3125 and 6.25 mg kg^{-1} body weight, respectively. The NIR laser irradiation was implemented for 5 min at 1 W cm^{-2} after the treatment for 24 h. The treatment groups from 1 to 12 are PBS, PBS + Laser, PCL-AuNC/Fe(OH)$_3$-PAA (JNPs), PCL-AuNC/Fe(OH)$_3$-PAA JNPs + Laser (JNPs + Laser), free Dox, free Dtxl, free Dox and free Dtxl (Dtxl/Dox), Dox loaded PCL-AuNC/Fe(OH)$_3$-PAA JNPs (Dox/JNPs), Dtxl loaded PCL-AuNC/Fe(OH)$_3$-PAA JNPs (Dtxl/JNPs), Dox loaded PCL-AuNC/Fe(OH)$_3$-PAA JNPs + Dtxl loaded PCL-AuNC/Fe(OH)$_3$-PAA JNPs (cocktail), Dtxl and Dox co-loaded PCL-AuNC/Fe(OH)$_3$-PAA JNPs (Dtxl/Dox/JNPs), and Dtxl and Dox co-loaded PCL-AuNC/Fe(OH)$_3$-PAA JNPs + Laser (Dtxl/Dox/JNPs + Laser), respectively.

The body weights of mice and tumor sizes were monitored every two days for 11 days. The tumor volume was calculated according to Equation (7):

$$\text{Volume} = \left(\frac{\text{length} \times \text{width}^2}{2}\right) \quad (7)$$

At day 11, mice from each group were randomly chosen and euthanized to retrieve tumors and organs. Tumor growth inhibition rate was determined using the following Equation (8):

$$\text{Inhibition}(\%) = \left(\frac{C - T}{C}\right) \times 100\% \quad (8)$$

where C is the average tumor weight of the control group and T is the average tumor weight of each treated group.

2.18. Histology examination and blood analysis

Ten of the healthy mice were randomly divided into two groups (n = 5, each group), which were treated by tail vein injection of PCL-AuNC/Fe(OH)$_3$-PAA JNPs (0.3 mg mL^{-1}, 200 μL) and PBS (200 μL) as control. Approximately 0.8 mL of blood from each mouse was collected for a blood chemistry test and complete blood panel analysis before the mouse was euthanized. The tissue sections of different organs were collected after the animals were sacrificed, and stained with hematoxylin&eosin (H&E). The digital microscope was used to examine all the sections.

3. Results and discussion

3.1. Synthesis and characterization of PCL-AuNC/Fe(OH)$_3$-PAA JNPs

The cubic AgNCs with about 60 nm were synthesized by a reported protocol (Fig. 1A) [47]. Then, we mixed the obtained AgNCs with PAA,

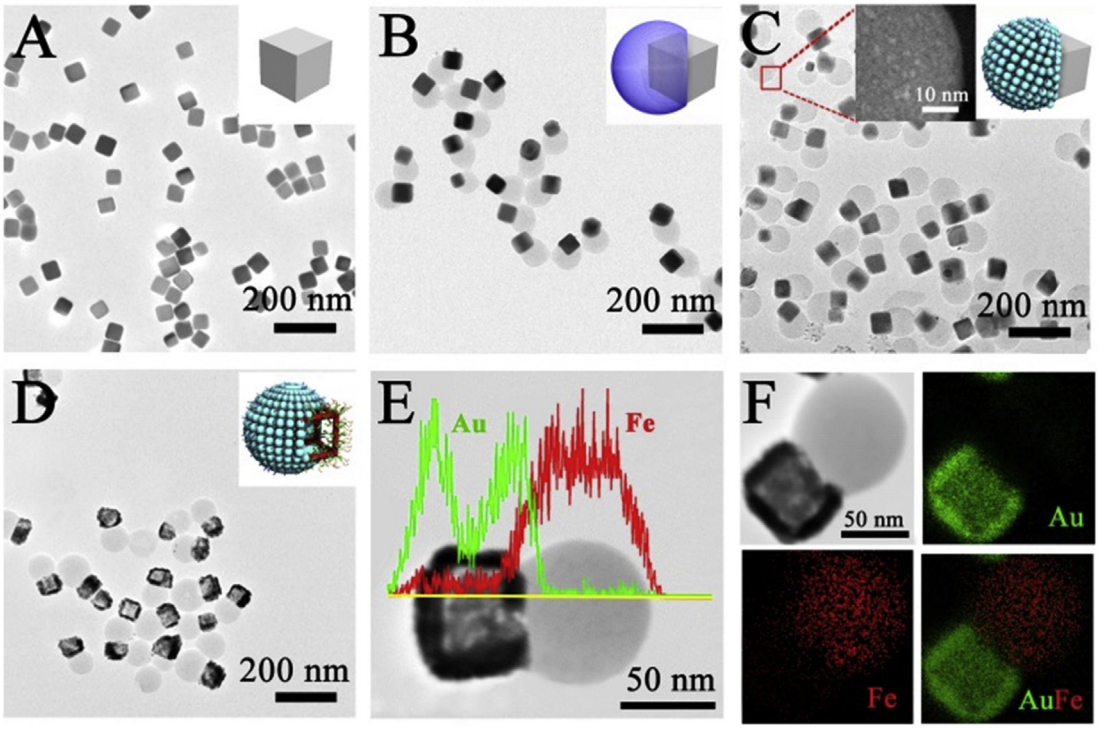

Fig. 1. TEM images of (A) AgNCs, (B) AgNC/PAA JNPs, (C) AgNC/$Fe(OH)_3$-PAA JNPs and (D) AuNC/$Fe(OH)_3$-PAA JNPs. The inset in (C) is the magnified SEM image of the surface of $Fe(OH)_3$-PAA domain. (E) Elemental line scan and (F) elemental mapping of a single AuNC/$Fe(OH)_3$-PAA JNP, respectively.

aqueous ammonium hydroxide in water. After the addition of isopropyl alcohol (IPA), the uniform cubic-sphere like AgNC/PAA JNPs precursors of ~120 nm were easily obtained through the change of the interfacial energy $\sigma_{AgNC\text{-}PAA}$, $\sigma_{AgNC\text{-}solvent}$, and $\sigma_{PAA\text{-}solvent}$ (Fig. 1B). In this process, the interfacial energy changed with the addition of IPA, resulting in $S = \sigma_{Ag\text{-}solvent} - (\sigma_{Ag\text{-}PAA} + \sigma_{PAA\text{-}solvent}) < 0$, where S is the spreading coefficient. Therefore, the partial engulfing of Ag was occurred and AgNC/PAA JNPs were obtained [45,46]. In addition, different sizes of coating PAA on the AgNCs can be easily prepared by changing the amount of PAA (Figure S1), which is in favor of further adjusting of drug loading. As we know, Fe is an essential mineral and an important component of proteins in the human body. Moreover, to endow the JNPs with independent storage and imaging capacity, the PAA part was selectively grown $Fe(OH)_3$ with about 60 nm by adding $FeCl_2{\cdot}4H_2O$ into the AgNC/PAA JNPs solution (Fig. 1C). In this reaction, PAA reserves water molecular inside its network to act as a nanoreactor, hence the Fe^{2+} can alternatively hydrolyze in this part to get.

$Fe(OH)_3$-PAA consisted of multiple small $Fe(OH)_3$ NPs. The rough surface could be observed from the magnified scanning electron microscope (SEM) imaging in the inset in Fig. 1C. The linear scan and elemental mapping carried by scanning transmission electron microscopy (STEM) imaging further confirmed their constitution and Janus nanostructure (Figure S2). The above reaction is quite repeatable, assuring the future scale-up. The resulted AgNC/$Fe(OH)_3$-PAA JNPs possess not only hydrophilic drug loading capacity, but also T_1 contrast-enhanced capability rooted from the 5 unpaired electrons in ferric ions (Fe^{3+}) for MRI. Subsequently, the other AgNC part of the AgNC/$Fe(OH)_3$-PAA JNP was etched with addition of $HAuCl_4$ to form the AuNC via the galvanic replacement reaction, which simultaneously had strong interaction with X-rays for effective CT imaging and the hollow interiors for accommodation of hydrophobic drug, as well as the NIR optical property (Fig. 2A). The finally obtained AuNC/$Fe(OH)_3$-PAA JNPs show obvious asymmetric Janus nanostructure with uniform size about 120 nm, consisting of a ~60 nm hollow AuNC and ~60 nm sphere like $Fe(OH)_3$-PAA (Fig. 1D). Linear scan implemented with STEM imaging across a single AuNC/$Fe(OH)_3$-PAA JNP displays a doughty Fe concentration on the right side of the whole JNP, and a higher Au concentration on the left side, as well as the hollow interior structure of AuNC with additional evidence provided by Au intensity (Fig. 1E). In addition, we can obviously observe from the elemental mapping on a randomly selected AuNC/$Fe(OH)_3$-PAA JNP that the JNP is composed of Au (Green) and Fe (red) in distinct sections, which is very consistent with the designed Janus nanostructure.

(Fig. 1F). Besides, the high resolution X-ray photoelectron spectroscopy (XPS) spectrum present the peaks at 83.8 and 87.4 eV are contributed to Au $4f_{1/2}$ and Au $4f_{5/2}$, respectively (Fig. 2B), while the peaks centered at 710.3 and 724.3 eV denote the Fe $2p_{3/2}$ and Fe $2p_{1/2}$ (Fig. 2C), further confirming the existence of Au and Fe in the AuNC/Fe$(OH)_3$-PAA JNPs. Furthermore, the exactly percentage of Au and Fe are 8.1 and 5.3 wt%, respectively, measured by an inductively coupled plasma (ICP). It is worth to mention that this method can be extended to synthesize other AgNC/X-PAA and AuNC/X-PAA (X represents silicon dioxide (SiO_2) or hydroxide gadolinium ($Gd(OH)_3$) JNPs (Figure S3), which may greatly expand the application of the AgNC and AuNC based JNPs.

In the present proof-of-concept study, the AuNC/$Fe(OH)_3$-PAA JNPs are designed to load hydrophilic and hydrophobic drugs in distinguished $Fe(OH)_3$-PAA and AuNC domains, respectively. However, pure AuNCs can not effectively load and preserve enough hydrophobic drugs. Hence, we choose the US Food and Drug Administration (FDA) approved PCL, which is hydrophobic enough to carry the hydrophobic drugs based on the principle of "like dissolves like", as the precursor to synthesize the PCL-SH via ring-opening polymerization using bis(2-hydroxyethyl)disulfide (HES) as an initiator followed by reduction with tributyl phosphine to modify AuNC [48]. The fourier transform infrared (FTIR) in Figs. 2D and ^{1}H NMR measurements in Fig. 2E were used to confirm the successful preparation and modification. ^{1}H NMR spectrum presents the characteristic peaks of methylene protons next to the thiol end group ($-CH_2-SH$) at δ 2.75 and the ^{1}H NMR end group analysis shows that the number of repeating units is 32, and the Mw can be deduced as about 3600. In Fig. 2Da, the FTIR characteristic peak at 1725 cm^{-1} is assigned to the polyester group of the neat PCL, and the

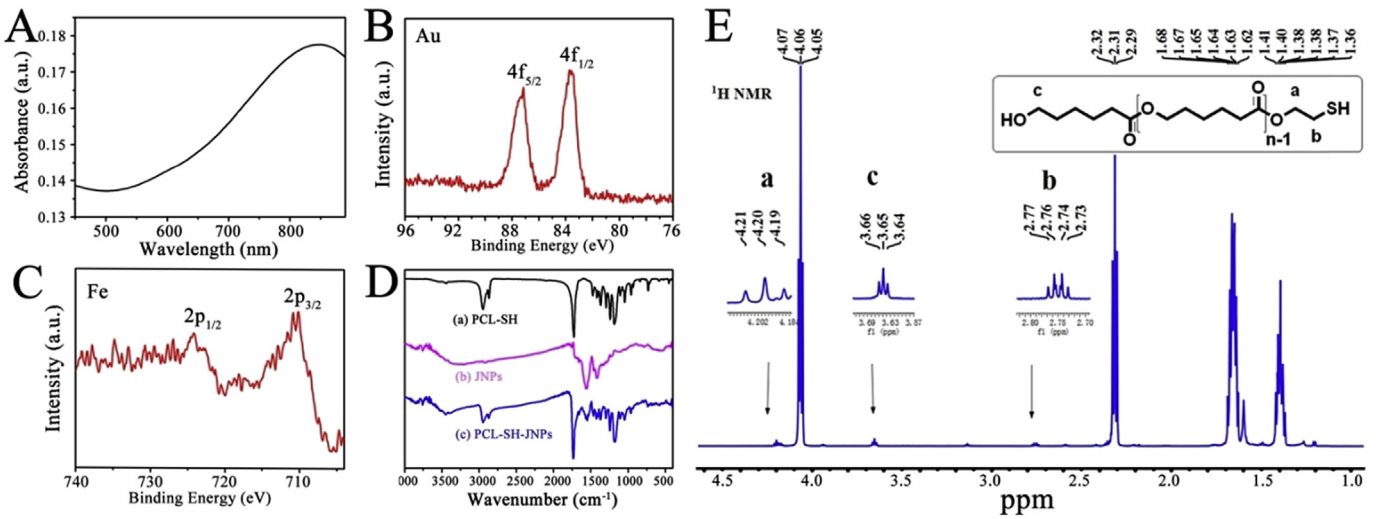

Fig. 2. (A) UV–Vis absorption spectrum of AuNC/Fe(OH)$_3$-PAA JNPs solution. (B) and (C) High resolution XPS spectra of AuNC/Fe(OH)$_3$-PAA JNPs. (D) FTIR spectra of PCL-SH, AuNC/Fe(OH)$_3$-PAA JNPs and PCL-AuNC/Fe(OH)$_3$-PAA JNPs. (E) ^{1}H NMR spectrum of PCL-SH.

vibrational band at 1557 cm^{-1} in Fig. 2Db is attributable to the stretching mode of the carboxyl C═O, indicating the presence of PAA. The coexistence of these two peaks in Fig. 2Dc demonstrates the successful modification of PCL-SH on the AuNC/Fe(OH)$_3$-PAA JNPs. After modification, we tested the hydrophobic drug loading capability by mixing docetaxel (Dtxl) with PCL-AuNC/Fe(OH)$_3$-PAA JNPs for 24 h and the loading capacity was about 5 wt%. To insure the stability of the PCL-AuNC/Fe(OH)$_3$-PAA JNPs after drug loading, methoxy-poly(ethylene glycol)-thiol (SH-PEG) was employed to further modify on the surface of AuNC. No precipitation of PEG-modified PCL-AuNC/Fe(OH)$_3$-PAA JNPs in water, PBS, culture medium or FBS could be observed within 4 h, suggesting their good stability (Figure S4). Afterward, the hydrophilic drug doxorubicin (Dox) was added and stored in the Fe(OH)$_3$-PAA part through the electrostatic attraction between the electropositive Dox and electronegative PAA, the loading capacity could reach to 20 wt%. As mentioned before, the negative charged PAA networks bearing carboxylate anions on PAA Chains encapsulated into the JNPs can bond positively charged Dox, therefore, when the more PAA exists in our JNPs, the more Dox loading capacity can be obtained (Table S1). As a result, the Dox loading content can be adjusted by using the PCL-AuNC/Fe(OH)$_3$-PAA JNPs with different sizes of Fe(OH)$_3$-PAA, thus regulating the ratio of the drugs (Dtxl:Dox) in each JNP. The successful control of the drug to drug ratio is a big step forward, which can govern the efficacy of combination treatment, especially for personalized therapy.

3.2. Photothermal performance

As displayed in Fig. 2A, the localized surface plasmon resonance (LSPR) peak of PCL-AuNC/Fe(OH)$_3$-PAA JNPs is around 840 nm, which is beneficial for the next NIR stimuli-release and IR thermal imaging, as well as photothermal ablation. With NIR irradiation at 1 W cm^{-2} for 5 min, the temperature of the solution goes up to 42.4 °C even with a lower concentration (7.5 μg mL^{-1}), and raises as high as 80 °C at 60 μg mL^{-1} (Fig. 3A). In contrast, the water just increases by 1.3 °C, suggesting that our JNPs make the significant contribution for the temperature increase. All the process was recorded by an infrared camera (Fig. 3B). Meanwhile, we test the cycle performance of the JNPs. As present in Fig. 3C, the highest temperature of the PCL-AuNC/Fe(OH)$_3$-PAA JNPs solution changed slightly (< 2 °C) in 4 cycle repeated NIR irradiation, demonstrating their better photostability and constant photothermal conversion behavior. After irradiation, there is no aggregation observed in solution, and there is almost no change in the morphology of PCL-AuNC/Fe(OH)$_3$-PAA JNPs observed from the TEM image (Figure S6). In this system, the photothermal conversion efficiency (η) of our JNPs is determined as 63% (Figure S5), which is the same as pure AuNCs and superior than most of the reported Au nanomaterials (Table S2) [44,49–51]. *In vitro* experiments show that there is almost no HepG-2 cell death in solo JNPs and NIR laser treated groups (Fig. 3D), but a high thermal contrast could be visually observed in the NIR laser irradiated PCL-AuNC/Fe(OH)$_3$-PAA JNPs treated group (Fig. 3E) and no cells is alive in this region (Fig. 3D), proposing their efficient transition from optical energy to heating, thus inducing cell ablation. From the *in vivo* experiments, we can also observe that the temperature in tumor site increases obviously with the enhancement of the time under NIR laser irradiation in the JNPs treated groups, compared to the PBS treated group (Fig. 3F). These results clearly indicate that our PCL-AuNC/Fe(OH)$_3$-PAA JNPs have excellent photothermal conversion capability for prospective inhibition of tumor growth.

3.3. In vitro dual drug release and defect on drug release sequence

It is well known that the two drugs preserved nanocarriers have the ability to deliver the drugs to the desire tumor site, overcoming the imparity of pharmacokinetics of different drugs. In addition, the schedule of administrated drug order is also important to determine the drug synergism and side effects [12,52]. As such, we design these unique PCL-AuNC/Fe(OH)$_3$-PAA JNPs, which allows for loading two drugs in its independent domains and releasing them by different stimulus respectively, benefited for us to investigate the therapeutic effect on release orders (Fig. 4A). Initially, we studied the independent stimuli-responsive property. As shown in Fig. 4B, the release profiles of Dtxl in neutral PBS and acidic PBS are almost the same, evidenced that the release of hydrophobic drug is a normally persistent tardiness process due to their hydrophobicity and the interaction with JNPs, and it takes about several days to reach a relatively high releasing value at physiological pH. While, only slight of Dox releases in neutral PBS, but 4 times higher release can be reached by changing the pH to acidity. The pH stimuli release of Dox is because that PAA is a pH sensitive polymer and Fe(OH)$_3$ NPs are not stable in acidic environment, hence, the Dox can easily escape from the broken Fe(OH)$_3$-PAA part and a burst release is observed. In Fig. 4C, with NIR laser irradiation at 0.5 W cm^{-2} for 5 min, the release of Dtxl in pH 7.4 and pH 5.3 increased obviously, but the release profiles of Dox in pH 7.4 and pH 5.3 are almost not changed, compared with none NIR laser group in Fig. 4B. When higher NIR laser power density (0.7 W cm^{-2} and 1 W cm^{-2},

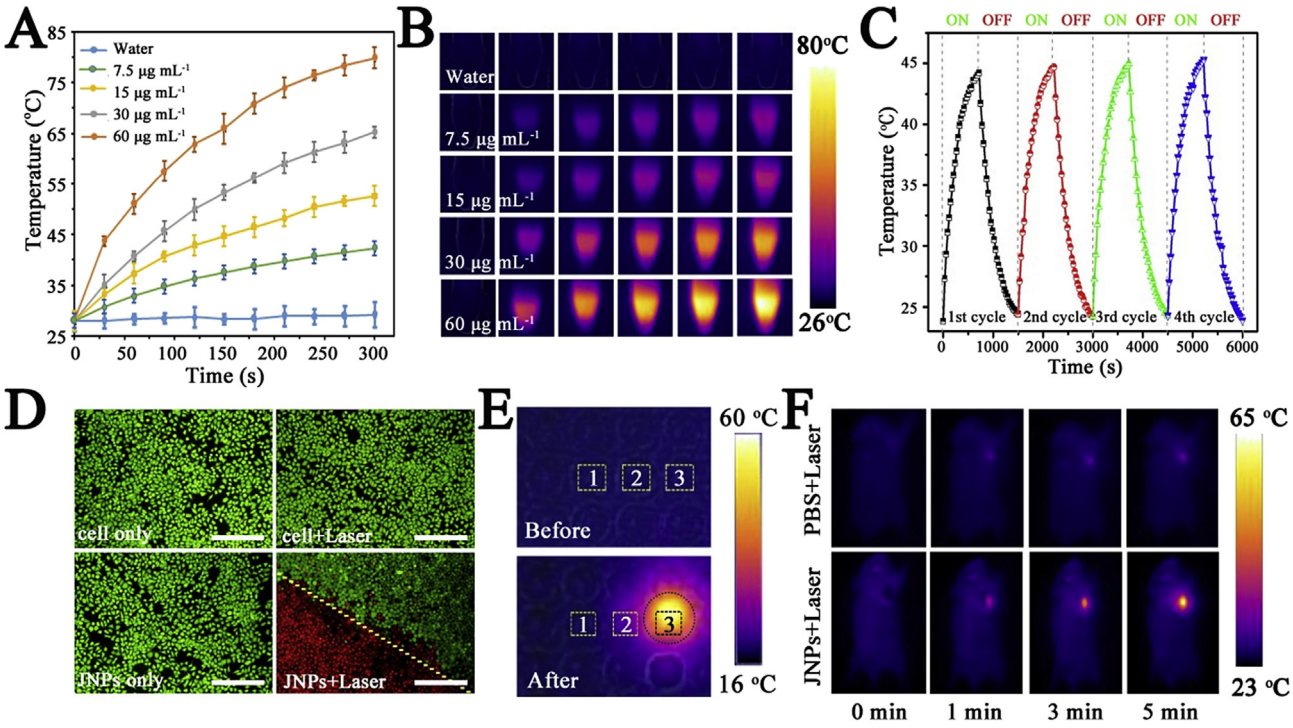

Fig. 3. (A) The temperature curves of water and PCL-AuNC/$Fe(OH)_3$-PAA JNPs with different concentrations, (B) and the corresponding IR thermal images. (C) Photostability of PCL-AuNC/$Fe(OH)_3$-PAA JNPs solution irradiated by NIR laser for 4 ON/OFF cycles. (D) Fluorescence microscopy investigation of calcein AM/PI stained HepG-2 cells treated with PBS, NIR laser, PCL-AuNC/$Fe(OH)_3$-PAA JNPs, and PCL-AuNC/$Fe(OH)_3$-PAA JNPs plus NIR laser. The scale bars represent 100 μm. (E) IR thermal images of the cell-culture plate containing PCL-AuNC/$Fe(OH)_3$-PAA JNPs treated cells (well no.1), cell only (well no.2), and PCL-AuNC/$Fe(OH)_3$-PAA JNPs treated cells under NIR laser (well no.3), where the irradiated region is marked by the circle. (F) IR thermal images of H-22-tumor-bearing BALB/c mice exposed to PBS and PCL-AuNC/$Fe(OH)_3$-PAA JNPs with NIR laser irradiation. The 808 nm NIR laser was irradiated for 5 min at 1 W cm^{-2}.

5 min) was implement, the total release amount of Dtxl increase slightly in pH 7.4 and pH 5.3, and the NIR laser effect on release of Dox appeared (Fig. 4D and E). We further exam the temperature change of the JNPs at different NIR laser power density (Fig. 4F), the stronger NIR laser power density was used, the higher temperature could be reached. Hence we guess the interesting phenomenon on the drug release is because that weak NIR laser irradiation (0.5 W cm^{-2}) induces higher heating inner AuNCs than $Fe(OH)_3$-PAA domain [53], which decreases the viscosity and increases the solubility of Dtxl inside AuNCs, as well as detachment of thio-PCL from JNPs [54,55], leading to the accelerated release of Dtxl but with less affect the release of Dox in $Fe(OH)_3$-PAA domain. The stronger NIR laser irradiation induce much higher heat in both AuNCs and $Fe(OH)_3$-PAA domains, hence the release of both drugs can be observed. Consequently, thanks to the flexibility of the extraordinary JNPs, the release of Dox and Dtxl can be controlled by pH and NIR laser irradiation with lower power density, respectively, which makes the optional sequential release possible. Therefore, we further explore their effect on cancer treatment. The CCK-8 results show that the blank JNPs with different concentrations are almost nontoxic (Figure S7). As shown in the assessment schedule in Fig. 4G, the HepG-2 cells were treated with Dtxl and Dox co-loaded PCL-AuNC/$Fe(OH)_3$-PAA JNPs (defined as Dtxl/Dox/JNPs) for 30 min and subsequently implemented NIR laser irradiation at different time points (0, 2, 6, 12, 24 and 48 h) over a period of 48 h, the cell cytotoxicity was then detected. JNPs and NIR laser only groups were also determined. No cytotoxicity was found in pure JNPs and NIR laser only groups. But, the cell viability is obviously different among all the Dtxl/Dox/JNPs under NIR laser irradiation groups, and the lowest cell viability is observed at 2 h compared to other NIR irradiation points. When the Dox loaded NPs were uptake by the lysosome or endosome in cytoplasm, which possess lower pH value, the Dox will release very quickly, but the Dtxl can not come out from the JNPs sufficiently. When the NIR laser irradiation was carried out at this point, it promoted the release of Dtxl, inducing the synchronous release of two drugs. If the irradiation was implement after 6 h, the Dox might release completed, which makes the programmed sequential release (Dox and Dtxl). From the cell viability results, the NIR laser irradiate at 2 h induces about 5% better therapeutic effect than other irradiation point. We speculate that this synchronous release may unify the pharmacokinetics of different drugs by simultaneously delivering and releasing dual drugs at the target site, thus enhance the curative effect and possibility of bench-to-bedside translation. Consequently, as a dual drug delivery system, the controlled release of each drug is a crucial important evaluation index, because the change of the drug release sequence will provide better cancer treatment, which holds great promise to overcome cancer drug resistance and bring new hope to cancer patients.

3.4. Biocompatibility and in vitro combined cancer therapy

Next, we evaluated the combination effect of dual drug loaded PCL-AuNC/$Fe(OH)_3$-PAA JNPs plus NIR laser to inhibit the proliferation of HepG-2 liver cancer cells. In Fig. 5A, the Dtxl/Dox/JNPs treated group shows more significant inhibition effect as compared to the solo drug loaded JNPs (Dox/JNPs or Dtxl/JNPs) groups. While, even compared with the cocktail (Dox loaded JNPs/Dtxl loaded JNPs) group, the dual drug loaded system still presents higher cytotoxicity. This is might because of the different release behavior of Dox/HCPT/JNPs and cocktail administration groups, indicating the superiority of synchronous release of drugs in dual drug co-loaded group. To exactly quantify the synergistic effect, the combination index (CI) is introduced, where the CI value is higher, equal or lower than 1 denoted the synergism, additivity, or antagonism, respectively. Firstly, the half maximal inhibitory concentrations (IC50) of Dox/JNPs, Dtxl/JNPs, Dtxl/Dox/JNPs and cocktail groups are calculated as 2.67, 2.43, 0.54 and

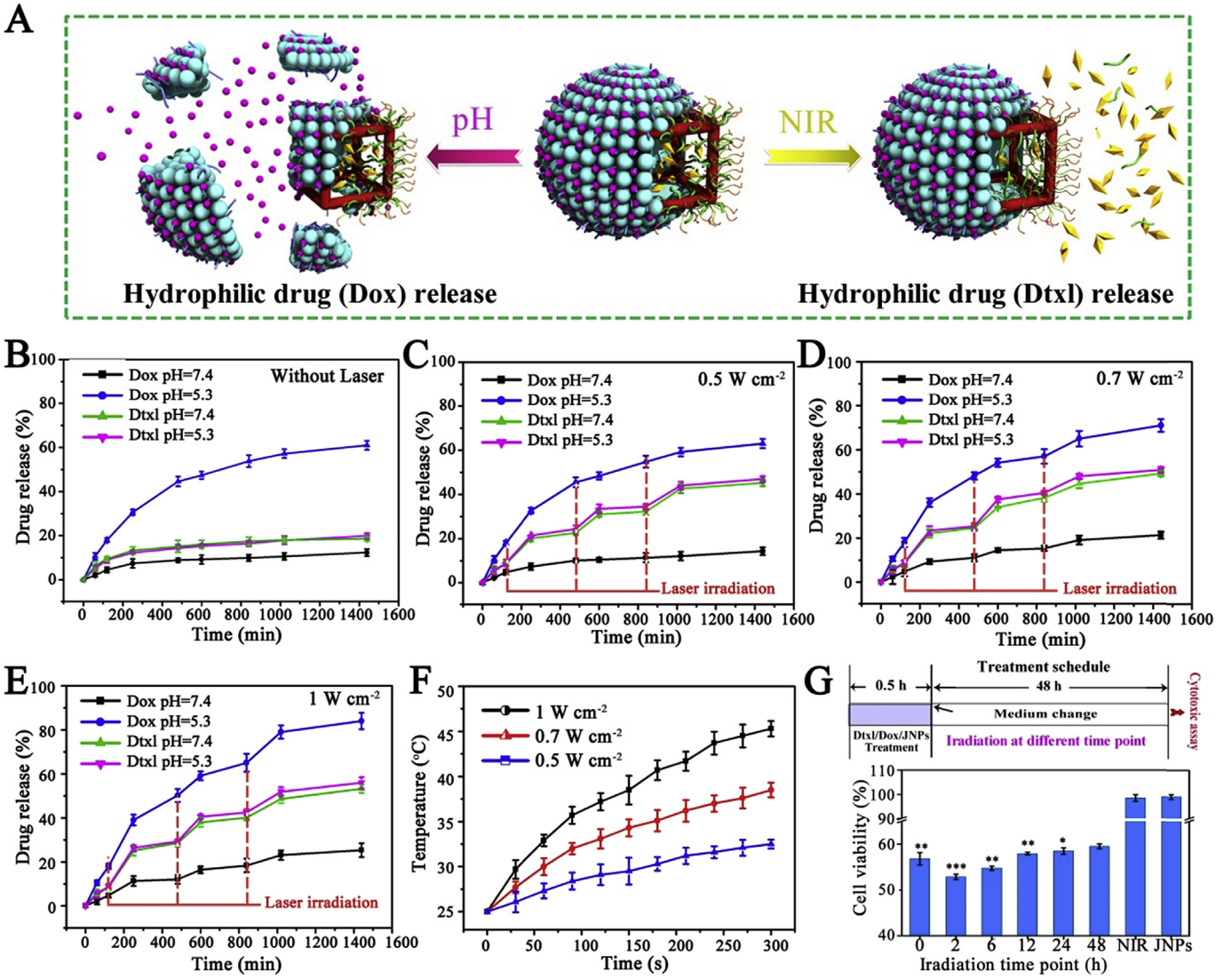

Fig. 4. (A) Schematic presentation for independent pH and NIR controlled release of Dtxl and Dox, respectively, by using PCL-AuNC/$Fe(OH)_3$-PAA JNPs. (B–E) Release profiles of Dox and Dtxl in PBS (pH = 5.3), or in PBS (pH = 7.4) with and without NIR laser irradiation (0.5, 0.7, and 1 W cm^{-2}, 5 min) at different time points. (F) The temperature changes of PCL-AuNC/$Fe(OH)_3$-PAA JNPs with NIR laser irradiation at different densities. (G) Treatment schedule (top) and viability (bottom) of HepG-2 cells incubated with Dtxl/Dox/JNPs for 30 min, followed by NIR irradiation (0.5 W cm^{-2}, 5 min) at 0, 2, 6, 12, 24 or 48 h, for 48 h, respectively. Cell treated with JNPs only and NIR laser only groups were under same condition. Mean ± SD are shown. Statistical significance (*$p < 0.05$, **$p < 0.01$ and ***$p < 0.001$) was attained when compared with cell treated with Dtxl/Dox/JNPs for 30 min and NIR irradiation at 48 h.

0.91 μg mL^{-1}, respectively. According to the data, CI of dual drug loaded group and cocktail group was determined as 0.42 and 0.71, respectively, indicating the synergistic effect in these two groups. Obviously, co-delivery of dual drugs in one nanosystem induces better therapeutic effect than cocktail group, which may be because that dual drug loaded JNPs can deliver more consistent combination drug payloads compared to cocktail JNP system, therefore maximizing their combinatorial effect. To investigate the inhibitory mechanism, we explore the effect of JNPs, solo drug loaded JNPs, cocktail and Dtxl/Dox/JNPs on cell cycles (Fig. 5D and E). Compared with culture medium treated HepG-2 cells, the cell cycles keep steady when treated with pure JNPs, which means our JNPs do not affect the cell cycles. It can be observed that the Dtxl/JNPs treated HepG-2 cells presents increased G2/M phase compared with that of the control group, indicating that the Dtxl is successfully disturbed the microtubule function in the G2/M phase [56]. Meanwhile, the HepG-2 cells treated with Dox, which has a mechanism of action against DNA, is blocked in G2/M phase in this case [57,58]. In these two solo drug loaded groups, the percentage of apoptotic HepG-2 cells treated with Dtxl/JNPs and Dox/JNPs are determined to be 29.7% and 34.1%, respectively, which are higher than control (11.7%) and solo JNPs (15%) groups (Fig. 5F). When treated with Dtxl/Dox/JNPs, the G2/M phase obviously enhances and the apoptosis (47.3%) significantly raises up, compared to the remarkable G2/M phase arrest but less apoptosis in cocktail group (42.4%), which means dual drug loaded JNPs can induce synergistic therapeutic effect to strengthen the cytotoxicity. To further exam the photothermal effect combined with chemotherapy, the HepG-2 cells were treated with culture medium, JNPs and Dtxl/Dox/JNPs with and without NIR laser irradiation, followed by the detection of the cell viability (Fig. 5B). As expect, almost no cell death was observed in the pure JNPs with different concentration groups and pure NIR laser group. But higher cytotoxicity could be found in the Dtxl/Dox/JNPs treated groups, indicating the chemotherapeutic effect. Meanwhile, the JNPs with NIR laser irradiation at different concentrations groups also presented higher cytotoxicity compared with corresponding JNPs without NIR laser groups. Moreover, the JNPs with NIR laser irradiation at different densities were examed (Figure S8). We observed that the cell viability decreased when the NIR laser density increased. The results indicate

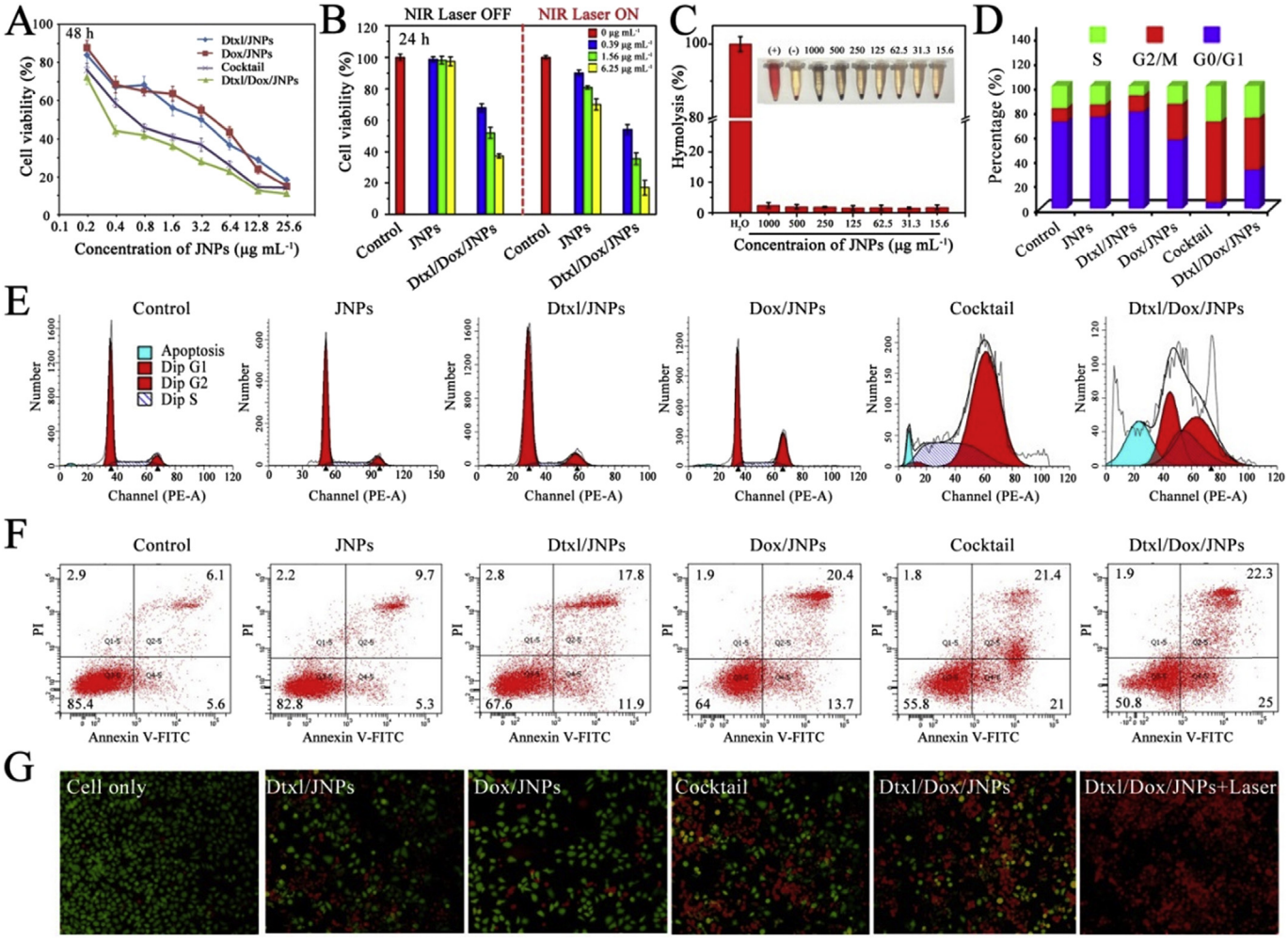

Fig. 5. (A) Viability of HepG-2 cells treated with Dtxl/JNPs, Dox/JNPs, cocktail and Dtxl/Dox/JNPs for 4 h and washed with fresh culture medium, then further incubated for another 44 h. (B) Cell viability of culture medium, JNPs and Dtxl/Dox/JNPs treated HepG-2 cells with and without NIR laser irradiation (1 W cm^{-2}, 5 min) for 24 h, respectively. (C) Hemolysis of PCL-AuNC/$Fe(OH)_3$-PAA JNPs, PBS (negative control) and deionized water (positive control) treated with red blood cells at various concentrations (0–1000 μg mL^{-1}) for 2 h, respectively. Inset is the hemolysis photo after centrifugation. (D) The relative changes in the percentage in each cell cycle phase and (E) the cell cycle distribution of HepG-2 cells induced by culture medium, JNPs, Dtxl/JNPs, Dox/JNPs, cocktail and Dtxl/Dox/JNPs with same drug concentrations, respectively. (F) Flow cytometry analysis for apoptosis of HepG-2 cells treated with culture medium, JNPs, Dtxl/JNPs, Dox/JNPs, cocktail and Dtxl/Dox/JNPs with same drug concentrations, respectively. Q1: necrotic cells, Q2: later apoptotic cells, Q3: living cells, Q4: early apoptotic cells. (G) Fluorescence microscopy investigation of calcein AM/PI stained HepG-2 cells treated with Dtxl/JNPs, Dox/JNPs, cocktail, Dtxl/Dox/JNPs and Dtxl/Dox/JNPs with NIR laser (1 W cm^{-2}, 5 min). (For interpretation of the references to color in this figure legend, the reader is referred to the Web version of this article.)

that the higher density of the NIR laser is irradiated, the more heat can be produced, thus inducing higher cytotoxicity, proved the effectiveness of the PPT by our PCL-AuNC/Fe(OH)3-PAA JNPs. Notably, when the Dtxl/Dox/JNPs treated cancer cells were subject to NIR laser for 5 min at 1 W cm^{-2}, the viability is remarkably decreased to 17% at concentration of 6.25 mg mL^{-1}, suggesting that the chemotherapy combined with photothermal therapy could cause more significant cytotoxicity. In addition, the HepG-2 cells with different treatments were stained by the calcein AM/PI and detected using fluorescence microscopy (Fig. 5G). It is evident that there are more red spots in the dual drug loaded JNPs treated group than the solo drug loaded JNPs groups and cocktail group, and almost no green spots can be observed in NIR laser irradiated group, which is coincide with the CCK-8 results. Hence, the enhancement in therapeutic behavior is not only due to the combination of two different drugs, but also because of the hyperthermia induced cancer cell ablation, which can effectively conquer the limitations of drug resistance and bio-toxicity. As mentioned, there is almost no cytotoxicity in blank JNPs treated cells. Likewise, the hemolysis experiment was carried out to further consider the biocompatibility of our JNPs. As shown in Fig. 5C, the calculated hemolysis ratio is less than 3% at the highest concentration (1000 μg mL^{-1}), manifesting that our JNPs are hemocompatible and can be administered intravenously for *in vivo* cancer treatment.

3.5. CT/MR bimodal imaging

To further increase the therapeutic accuracy and effect, the two separate segments of the PCL-AuNC/$Fe(OH)_3$-PAA JNPs are designed for CT and MR imaging, respectively. Owing to the high X-ray attenuation of Au element, our PCL-AuNC/$Fe(OH)_3$-PAA JNPs with different concentrations were implemented using a clinical CT scanner to acquire the CT images. As shown in Fig. 6A, the CT image contrast become significantly brighter and the HU values increase linearly as the JNPs concentration enhanced. After intravenous (i.v.) injection of our JNPs into BALB/c mouse bearing H-22 tumors for 24 h, the CT signal intensity in the tumor site recommends two-fold positive enhancement compared to the CT image before injection (Fig. 6B and C), indicating that these JNPs could act as a potential CT contrast agent for accurate location of the tumor *in vivo*. Although CT technique has already provided high resolution images, its lower sensitivity to the soft tissues is

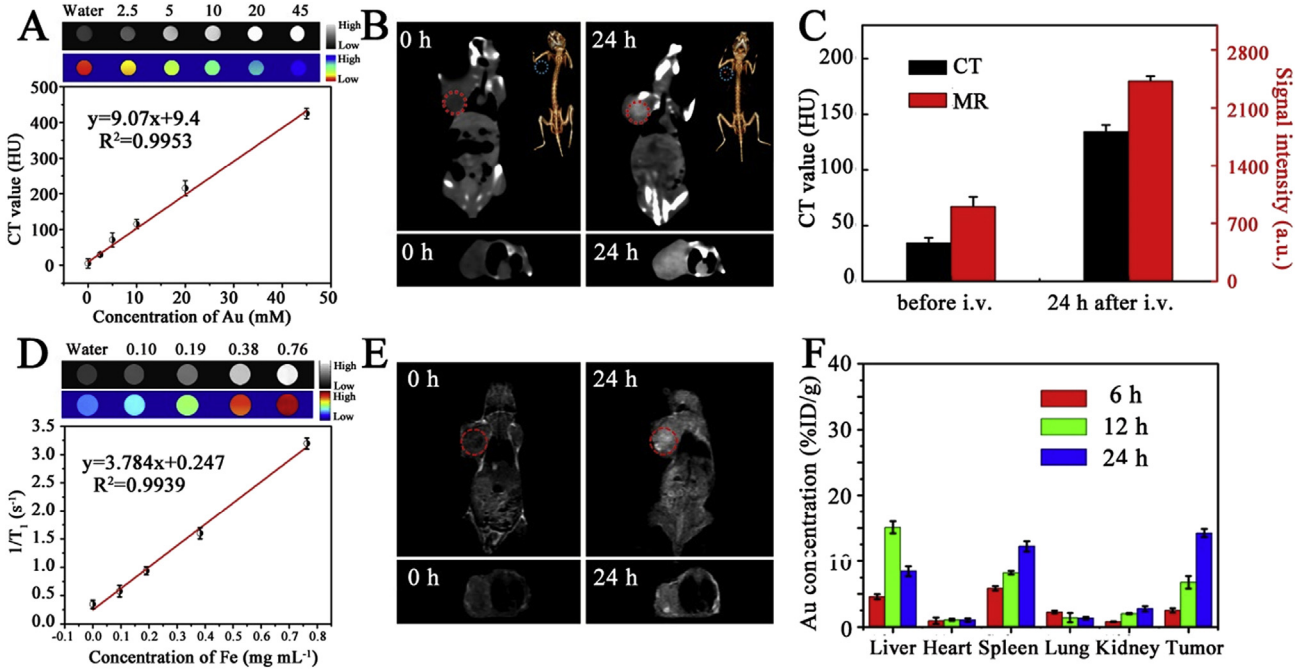

Fig. 6. (A) CT images and attenuation (HU) plot of PCL-AuNC/$Fe(OH)_3$-PAA JNPs with different concentrations *in vitro*. (B) Cross-sectional CT images of mouse collected pre- and 24 h post- intravenous (i.v.) injection. Inset is the corresponding 3D CT images. (C) CT values and MR signal intensity of mouse pre- and 24 h post-i.v. injection of PCL-AuNC/$Fe(OH)_3$-PAA JNPs. (D) MR images and plot of $1/T_1$ over Fe concentration of our PCL-AuNC/$Fe(OH)_3$-PAA JNPs. The slope means the specific relaxivity (r_1). (E) T_1 weighted MR images of mouse pre- and 24 h post- i.v. injection. (F) Quantitative measurement of Au concentrations in each organ of the mice after i.v. injection of PCL-AuNC/$Fe(OH)_3$-PAA JNPs for different times.

still a big restriction for further clinical application. Fortunately, the emergence of MRI has solved this problem, because it has lower resolution but higher sensitivity to soft tissues for non-ionizing radiation. As we know, T_1 contrast effect is induced by the interactions between protons of water molecules and electron spins of the contrast agent, since there are 5 unpaired electrons in ferric ions (Fe^{3+}), which is desirable as T_1 contrast agent. Therefore, a plenty of $Fe(OH)_3$ NPs in the other side of PCL-AuNC/$Fe(OH)_3$-PAA JNPs possess the potential capacity as T_1 weighted MR contrast. As expected, the T_1 weighted phantom images demonstrates that PCL-AuNC/$Fe(OH)_3$-PAA JNPs have much stronger positive contrast effect, and the relaxation rate is linearly with enhanced Fe concentration (Fig. 6D). The brightness observed at the tumor site also proves the higher tumor uptake of these JNPs at 24 h post injection (Fig. 6C and E). To further evaluate the tissue distribution of our JNPs at different times, the major organs (heart, liver, lung, spleen and kidney) and tumor were harvested and measured by ICP (Fig. 6F). The results manifest that the highest accumulation of PCL-AuNC/$Fe(OH)_3$-PAA JNPs in tumor site is after 24 h post injection due to the enhanced permeability and retention effect (EPR) effect compared to 6 and 12 h, which is in accordance with the CT and MR results. Thus, both CT and MR imaging results confirm the efficient tumor location of the PCL-AuNC/$Fe(OH)_3$-PAA JNPs, and further guide the *in vivo* experiment.

3.6. *In vivo synergistic chemo-photothermal therapy*

Finally, we applied the PCL-AuNC/$Fe(OH)_3$-PAA JNPs for *in vivo* combined chemo-photothermal therapy against BALB/c mice bearing H-22 liver cancer. The mice were divided into 12 groups (n = 7 per group) with different treatments: PBS, pure JNPs, free Dox, free Dtxl, free Dtxl and Dox (Dtxl/Dox), Dox/JNPs, Dtxl/JNPs, cocktail, PBS + laser, JNPs + laser, Dtxl/Dox/JNPs and Dtxl/Dox/JNPs + laser. The NIR laser was implemented 24 h post intravenous injection, because the ICP, CT and MRI results indicated that the higher accumulation of our JNPs was reached the at this point. Among all the groups, the body weight changes of the mice keep steady except the control group, which may be because of the growth of the tumors (Fig. 7A). Moreover, significant difference in the tumor volume is observed in 11 days (Fig. 7B), reflecting the therapeutic effect. To exactly acquire the results, all the tumors in the mice were collected and weighted to evaluate the inhibition rate (Fig. 7C and D). As shown in Fig. 7C, the mean tumor weight of the hydrophobic drug loaded group (Dtxl/JNPs) is obviously smaller than free drug group (free Dtxl). The weak restrain in free Dtxl treated group is due to the hydrophobic nature of the Dtxl, and the higher inhibition appeared in Dtxl/JNPs treated group is because of their accumulation in the desire tumor site by EPR effect once intravenously administered. For dual drug administration groups, the inhibition rates of Dtxl/Dox/JNPs, cocktail and free drug combination groups are all better than the single drug loaded JNPs groups, indicating the multi-drug combination is extremely effective. It is worth to mention that the cocktail administration of Dtxl/JNPs and Dox/JNPs group do not exhibit obvious tumor inhibition compared to dual drug administrated groups, probably because the improper sequential drug release lead to unintended cell cycle arrest and diminished response to the subsequent drug. Therefore, the above results manifest that the release of the Dtxl and Dox from the JNPs in a proper manner can obtain the synergistic therapeutic effect, but not in simply blending. Apart from the chemotherapy, we also applied PTT on the mice. As expected, the Dtxl/Dox/JNPs plus NIR laser induces fantastic tumor depression, and some of the tumors even disappeared, proving that our PCL-AuNC/$Fe(OH)_3$-PAA JNPs have brilliant ability to synergistically restrain tumor growth by integrating the chemo-photothermal therapy. We tested the biochemical indexes (Fig. 7E), including alanine transaminase (ALT), aspartate transaminase (AST), albumin (ALB), total protein (TP), total bilirubin (TBIL), blood urea nitrogen (BUN), creatinine (CRE) and uric acid (UA), which are related function indicators for the liver and kidney. No physiologically significant difference ($P > 0.05$) was observed between the two groups, indicating that the administration of the JNPs caused no obvious renal and hepatic dysfunction in mice. Furthermore, histological examination of hematoxylin

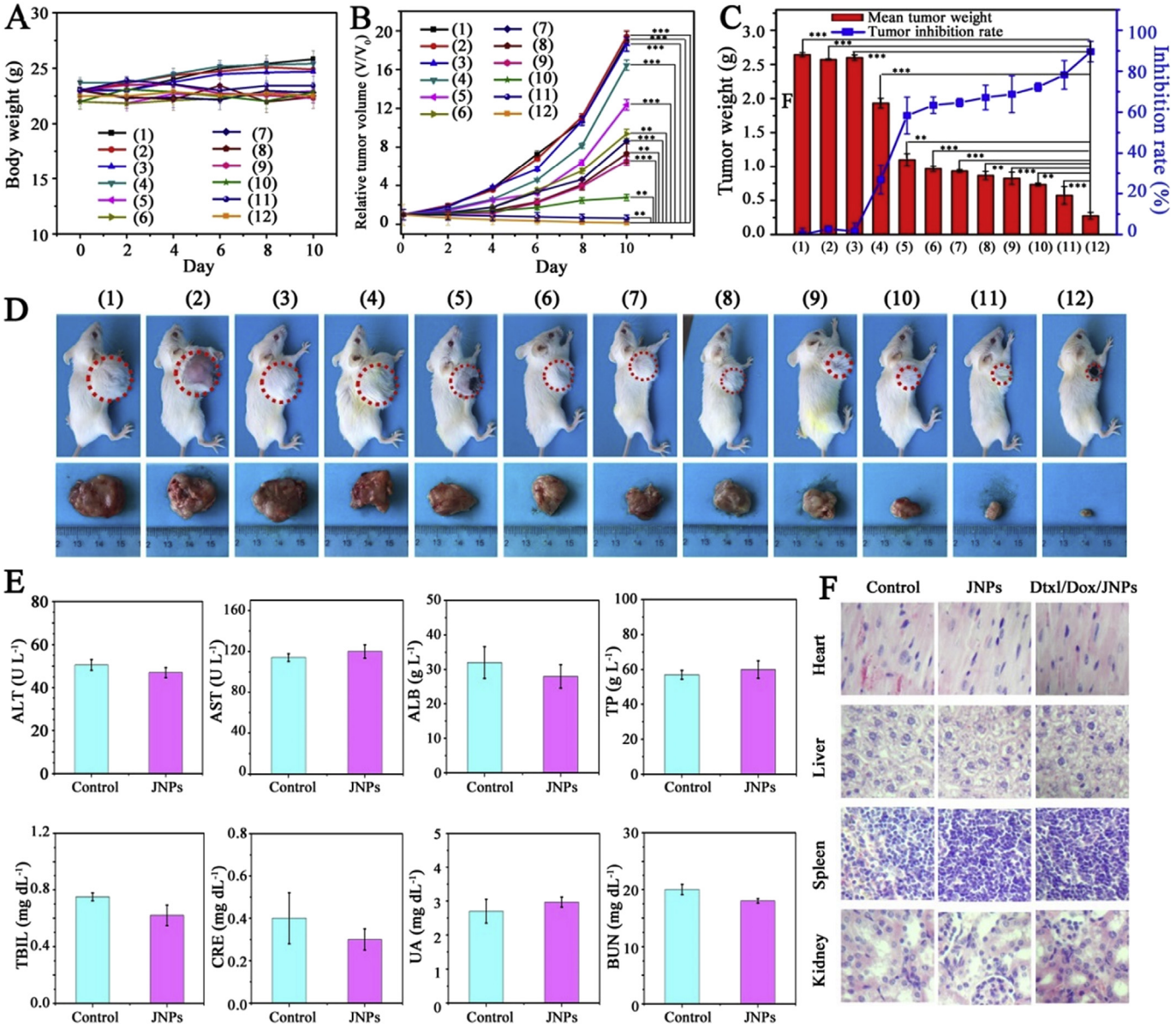

Fig. 7. Changes in (A) body weight and (B) relative tumor volume of H-22 bearing BALB/c mice with different treatments in 11 days. (C) Mean tumor weight and relative tumor inhibition rate of H-22 tumor bearing BALB/c mice with different treatments. (D) Representative photographs of mice and tumors with different treatments for chemo and photothermal therapy. The treatments from 1 to 12 represent PBS, PBS + Laser, pure JNPs, free Dtxl, JNPs + laser, free Dox, Dox/JNPs, Dtxl/JNPs, cocktail, free Dtxl and Dox (Dtxl/Dox), Dtxl/Dox/JNPs and Dtxl/Dox/JNPs + laser. (E) Blood biochemical indexes for the mice treated with PBS (control) and PCL-AuNC/Fe$(OH)_3$-PAA JNPs. (F) Histological section of major organ tissues stained with hematoxylin and eosin after post i.v. injection of PBS (control), PCL-AuNC/Fe$(OH)_3$-PAA JNPs and Dtxl and Dox co-loaded PCL-AuNC/Fe$(OH)_3$-PAA JNPs. Statistical significance:**$p < 0.01$, ***$p < 0.001$.

and eosin stained tissue sections of the major organs of PCL-AuNC/Fe$(OH)_3$-PAA JNPs and dual drug loaded PCL-AuNC/Fe$(OH)_3$-PAA JNPs treated groups show well-organized cell structure as that of the saline treated group (Fig. 7F). These results demonstrate that our unique JNPs are promising for precise cancer theranostics.

4. Conclusion

In summary, we designed and synthesized a unique cage-sphere like AuNC/Fe$(OH)_3$-PAA JNP for the first time with totally different morphologies, functionalities and surface properties in its two distinct sides, and further discuss their therapeutic effect of drug administrated order coupled with imaging-guided combined therapy. Firstly, we fabricated a novel cubic-sphere structural AgNC/PAA JNP as precursors, which was further used to selectively grow Fe$(OH)_3$ on the PAA domain, and subsequently etch to form AuNC on the AgNC side, finally obtained a unique cage-sphere like AuNC/Fe$(OH)_3$-PAA JNP with both NIR/pH stimuli-responsive properties and CT/MR imaging capacities, respectively. After modification with PCL-SH, the totally different hydrophobic and hydrophilic drugs (5% Dtxl and 20% Dox) were separately loaded into one PCL-AuNC/Fe$(OH)_3$-PAA JNP but two independent PCL-AuNC and Fe$(OH)_3$-PAA domains. Benefit from the extraordinary heterostructure and independent pH and NIR sensitive properties, the optional sequential drug release by an inorganic JNP was realized for the first time, and the results presented the synchronous release of two drugs had 5% better therapeutic effect. Moreover, the dual drug loaded PCL-AuNC/Fe$(OH)_3$-PAA JNPs with NIR laser irradiation induced the highest tumor inhibition, thanks to the synergistic chemo and photothermal therapy. Furthermore, the cubic-sphere like AgNC/PAA JNPs could be very interesting precursors for the

preparation of other new types of nanomaterials for various applications. Overall, the extraordinary cage-sphere structural PCL-AuNC/Fe$(OH)_3$-PAA JNP consist of two distinct segments with different functionalities provide a new concept and approach in the progress of cancer therapy.

Acknowledgements

Dr Lingyu Zhang and Manjie Zhang contribute equally to this work. The authors acknowledge helpful discussions with Dr. Danfeng Pei. The authors also thank Dr. Philippe Saint-Cricq-Riviere for suggestions and editing of the English. This project is financially supported by the NSFC (21603029, 21573040 and 21301027); Natural Science Foundation and Science and Technology Development Planning of Jilin Province, China (20170520148JH, 20150204086GX); China Postdoctoral Science Foundation (2016M600224); Jilin Provincial Research Foundation for Basic Research, China (20160519012JH); Jilin Provincial Key Laboratory of Advanced Energy Materials, China (Northeast Normal University); the Fundamental Research Funds for the Central Universities.

Appendix A. Supplementary data

Supplementary data related to this article can be found at https://doi.org/10.1016/j.biomaterials.2018.07.060.

References

[1] D. Peer, J.M. Karp, S. Hong, O.C. Farokhzad, R. Margalit, R. Langer, Nanocarriers as an emerging platform for cancer therapy, Nat. Nanotechnol. 2 (2007) 751–760.
[2] L. Zhang, F.X. Gu, J.M. Chan, A.Z. Wang, R.S. Langer, O.C. Farokhzad, Nanoparticles in medicine: therapeutic applications and developments, Clin. Pharmacol. Ther. 83 (2008) 761–769.
[3] L. Ma, M. Kohli, A. Smith, Nanoparticles for combination drug therapy, ACS Nano 7 (2013) 9518–9525.
[4] B.A. Chabner, T.G. Roberts Jr., Chemotherapy and the war on cancer, Nat. Rev. Canc. 5 (2005) 65–72.
[5] Y. Li, T. Thambi, D.S. Lee, Co-delivery of drugs and genes using polymeric nanoparticles for synergistic cancer therapeutic effects, Adv. Healthc. Mater. 7 (2018) 1700886-n/a.
[6] L. Liao, J. Liu, E.C. Dreaden, S.W. Morton, K.E. Shopsowitz, P.T. Hammond, et al., A convergent synthetic platform for single-nanoparticle combination cancer therapy: ratiometric loading and controlled release of cisplatin, doxorubicin, and camptothecin, J. Am. Chem. Soc. 136 (2014) 5896–5899.
[7] J.-C. Yang, Y. Chen, Y.-H. Li, X.-B. Yin, Magnetic resonance imaging-guided multidrug chemotherapy and photothermal synergistic therapy with ph and nir-stimulation release, ACS Appl. Mater. Interfaces 9 (2017) 22278–22288.
[8] D. Lu, M.G. Wientjes, Z. Lu, J.L.-S. Au, Tumor priming enhances delivery and efficacy of nanomedicines, J. Pharmacol. Exp. Therapeut. 322 (2007) 80–88.
[9] M.A. Shah, G.K. Schwartz, The relevance of drug sequence in combination chemotherapy, Drug Resist. Updates 3 (2000) 335–356.
[10] K.A. Janes, H.C. Reinhardt, M.B. Yaffe, Cytokine-induced signaling networks prioritize dynamic range over signal strength, Cell 135 (2008) 343–354.
[11] Z. Luo, S. Zhang, J. Pan, R. Shi, H. Liu, Y. Lyu, et al., Time-responsive osteogenic niche of stem cells: a sequentially triggered, dual-peptide loaded, alginate hybrid system for promoting cell activity and osteo-differentiation, Biomaterials 163 (2018) 25–42.
[12] X. Liang, C. Gao, L. Cui, S. Wang, J. Wang, Z. Dai, Self-assembly of an amphiphilic Janus camptothecin–floxuridine conjugate into liposome-like nanocapsules for more efficacious combination chemotherapy in cancer, Adv. Mater. 29 (2017) 1703135–n/a.
[13] C.E. Ashley, E.C. Carnes, G.K. Phillips, D. Padilla, P.N. Durfee, P.A. Brown, et al., The targeted delivery of multicomponent cargos to cancer cells by nanoporous particle-supported lipid bilayers, Nat. Mater. 10 (2011) 389–397.
[14] A. Landarani-Isfahani, M. Moghadam, S. Mohammadi, M. Royvaran, N. Moshtael-Arani, S. Rezaei, et al., Elegant ph-responsive nanovehicle for drug delivery based on triazine dendrimer modified magnetic nanoparticles, Langmuir 33 (2017) 8503–8515.
[15] Z. Zhao, S. Lou, Y. Hu, J. Zhu, C. Zhang, A nano-in-nano polymer–dendrimer nanoparticle-based nanosystem for controlled multidrug delivery, Mol. Pharm. 14 (2017) 2697–2710.
[16] P. Kesharwani, A.K. Iyer, Recent advances in dendrimer-based nanovectors for tumor-targeted drug and gene delivery, Drug Discov. Today 20 (2015) 536–547.
[17] M. Callari, S. Wong, H. Lu, J. Aldrich-Wright, P. De Souza, M.H. Stenzel, Drug induced self-assembly of triblock copolymers into polymersomes for the synergistic dual-drug delivery of platinum drugs and paclitaxel, Polym. Chem. 8 (2017) 6289–6299.
[18] H. Wang, Y. Zhao, Y. Wu, Y-l Hu, K. Nan, G. Nie, et al., Enhanced anti-tumor efficacy by Co-Delivery of doxorubicin and paclitaxel with amphiphilic methoxy pegplga copolymer nanoparticles, Biomaterials 32 (2011) 8281–8290.
[19] H. Baabur-Cohen, L.I. Vossen, H.R. Krüger, A. Eldar-boock, E. Yeini, N. Landa-Rouben, et al., In vivo comparative study of distinct polymeric architectures bearing a combination of paclitaxel and doxorubicin at a synergistic ratio, J. Contr. Release 257 (2017) 118–131.
[20] R. Zhao, T. Li, G. Zheng, K. Jiang, L. Fan, J. Shao, Simultaneous inhibition of growth and metastasis of hepatocellular carcinoma by Co-Delivery of ursolic acid and sorafenib using lactobionic acid modified and ph-sensitive chitosan-conjugated mesoporous silica nanocomplex, Biomaterials 143 (2017) 1–16.
[21] M. Chen, S. Yang, X. He, K. Wang, P. Qiu, D. He, Co-loading of coralyne and indocyanine green into adenine DNA-functionalized mesoporous silica nanoparticles for ph- and near-infrared-responsive chemothermal treatment of cancer cells, J. Mater. Chem. B 2 (2014) 6064–6071.
[22] H. Meng, M. Liong, T. Xia, Z. Li, Z. Ji, J.I. Zink, et al., Engineered design of mesoporous silica nanoparticles to deliver doxorubicin and P-Glycoprotein sirna to overcome drug resistance in a cancer cell line, ACS Nano 4 (2010) 4539–4550.
[23] X. Li, L. Zhou, Y. Wei, A.M. El-Toni, F. Zhang, D. Zhao, Anisotropic growth-induced synthesis of dual-compartment Janus mesoporous silica nanoparticles for bimodal triggered drugs delivery, J. Am. Chem. Soc. 136 (2014) 15086–15092.
[24] L. Zhang, Y. Chen, Z. Li, L. Li, P. Saint-Cricq, C. Li, et al., Tailored synthesis of Octopus-Type Janus nanoparticles for synergistic actively-targeted and chemo-photothermal therapy, Angew. Chem. Int. Ed. 128 (2016) 2158–2161.
[25] Z. Wang, D. Shao, Z. Chang, M. Lu, Y. Wang, J. Yue, et al., Janus gold nanoplatform for synergetic chemoradiotherapy and computed tomography imaging of hepatocellular carcinoma, ACS Nano 11 (2017) 12732–12741.
[26] L.M. Liz-Marzán, M. Grzelczak, Growing anisotropic crystals at the nanoscale, Science 356 (2017) 1120–1121.
[27] G. Song, M. Chen, Y. Zhang, L. Cui, H. Qu, X. Zheng, et al., Janus iron oxides @ semiconducting polymer nanoparticle tracer for cell tracking by magnetic particle imaging, Nano Lett. 18 (2018) 182–189.
[28] Y. Li, W. Li, W. Bao, B. Liu, D. Li, Y. Jiang, et al., Bioinspired peptosomes with programmed stimuli-responses for sequential drug release and high-performance anticancer therapy, Nanoscale 9 (2017) 9317–9324.
[29] S. Li, L. Zhang, T. Wang, L. Li, C. Wang, Z. Su, The facile synthesis of hollow Au nanoflowers for synergistic chemo-photothermal cancer therapy, Chem. Commun. 51 (2015) 14338–14341.
[30] Q. Wu, M. Niu, X. Chen, L. Tan, C. Fu, X. Ren, et al., Biocompatible and biodegradable zeolitic imidazolate framework/polydopamine nanocarriers for dual stimulus triggered tumor thermo-chemotherapy, Biomaterials 162 (2018) 132–143.
[31] D. Ni, J. Zhang, J. Wang, P. Hu, Y. Jin, Z. Tang, et al., Oxygen vacancy enables markedly enhanced magnetic resonance imaging-guided photothermal therapy of a Gd3+-Doped contrast agent, ACS Nano 11 (2017) 4256–4264.
[32] Y. Ju, H. Zhang, J. Yu, S. Tong, N. Tian, Z. Wang, et al., Monodisperse Au–Fe2c Janus nanoparticles: an attractive multifunctional material for triple-modal imaging-guided tumor photothermal therapy, ACS Nano 11 (2017) 9239–9248.
[33] Y. Xia, W. Li, C.M. Cobley, J. Chen, X. Xia, Q. Zhang, et al., Gold nanocages: from synthesis to theranostic applications, Acc. Chem. Res. 44 (2011) 914–924.
[34] G.D. Moon, S.-W. Choi, X. Cai, W. Li, E.C. Cho, U. Jeong, et al., A new theranostic system based on gold nanocages and phase-change materials with unique features for photoacoustic imaging and controlled release, J. Am. Chem. Soc. 133 (2011) 4762–4765.
[35] J. Zeng, L. Jing, Y. Hou, M. Jiao, R. Qiao, Q. Jia, et al., Anchoring group effects of surface ligands on magnetic properties of Fe3o4 nanoparticles: towards high performance mri contrast agents, Adv. Mater. 26 (2014) 2694–2698.
[36] C. Liang, J. Dawei, K. Anyanee, F. VH, I. Hyung-Jun, F. Liangzhu, et al., Renal-clearable pegylated porphyrin nanoparticles for image-guided photodynamic cancer therapy, Adv. Funct. Mater. 27 (2017) 1702928.
[37] J. Yang, D. Shen, L. Zhou, W. Li, X. Li, C. Yao, et al., Spatially confined fabrication of core–shell gold Nanocages@Mesoporous silica for near-infrared controlled photothermal drug release, Chem. Mater. 25 (2013) 3030–3037.
[38] P. Shi, K. Qu, J. Wang, M. Li, J. Ren, X. Qu, Ph-responsive nir enhanced drug release from gold nanocages possesses high potency against cancer cells, Chem. Commun. 48 (2012) 7640–7642.
[39] G. Yang, L. Xu, Y. Chao, J. Xu, X. Sun, Y. Wu, et al., Hollow Mno2 as a tumor-microenvironment-responsive biodegradable nano-platform for combination therapy favoring antitumor immune responses, Nat. Commun. 8 (2017) 902.
[40] Y. Chang, Y. Cheng, Y. Feng, H. Jian, L. Wang, X. Ma, et al., Resonance energy transfer-promoted photothermal and photodynamic performance of gold–copper sulfide yolk–shell nanoparticles for chemophototherapy of cancer, Nano Lett. (2018), https://doi.org/10.1021/acs.nanolett.7b04162.
[41] C. Wang, C. Xu, L. Xu, C. Sun, D. Yang, J. Xu, et al., A novel core-shell structured upconversion nanorod as a multimodal bioimaging and photothermal ablation agent for cancer theranostics, J. Mater. Chem. B 6 (2018) 2597–2607.
[42] W. Fan, B. Yung, P. Huang, X. Chen, Nanotechnology for multimodal synergistic cancer therapy, Chem. Rev. 117 (2017) 13566–13638.
[43] Y. Yu, Z. Wenjun, D. Ziliang, C. Yu, X. Lai, C. Meiwan, et al., 1d coordination polymer nanofibers for low-temperature photothermal therapy, Adv. Mater. 29 (2017) 1703588.
[44] P. Huang, J. Lin, W. Li, P. Rong, Z. Wang, S. Wang, et al., Biodegradable gold nanovesicles with an ultrastrong plasmonic coupling effect for photoacoustic imaging and photothermal therapy, Angew. Chem. Int. Ed. 125 (2013) 14208–14214.
[45] L. Li, L. Zhang, S. Xing, T. Wang, S. Luo, X. Zhang, et al., Generalized approach to the synthesis of reversible concentric and eccentric polymer-coated nanostructures, Small 9 (2013) 825–830.

[46] S. Torza, S.G. Mason, Three-phase interactions in shear and electrical fields, J. Colloid Interface Sci. 33 (1970) 67–83.
[47] S.E. Skrabalak, L. Au, X. Li, Y. Xia, Facile synthesis of Ag nanocubes and Au nanocages, Nat. Protoc. 2 (2007) 2182–2190.
[48] H. Sun, B. Guo, R. Cheng, F. Meng, H. Liu, Z. Zhong, Biodegradable micelles with sheddable poly(ethylene glycol) shells for triggered intracellular release of doxorubicin, Biomaterials 30 (2009) 6358–6366.
[49] C.M. Hessel, V.P. Pattani, M. Rasch, M.G. Panthani, B. Koo, J.W. Tunnell, et al., Copper selenide nanocrystals for photothermal therapy, Nano Lett. 11 (2011) 2560–2566.
[50] P. Huang, P. Rong, J. Lin, W. Li, X. Yan, M.G. Zhang, et al., Triphase interface synthesis of plasmonic gold bellflowers as near-infrared light mediated acoustic and thermal theranostics, J. Am. Chem. Soc. 136 (2014) 8307–8313.
[51] J. Zeng, D. Goldfeld, Y. Xia, A plasmon-assisted optofluidic (paof) system for measuring the photothermal conversion efficiencies of gold nanostructures and controlling an electrical switch, Angew. Chem. Int. Ed. 52 (2013) 4169–4173.
[52] F.A. Holmes, T. Madden, R.A. Newman, V. Valero, R.L. Theriault, G. Fraschini, et al., Sequence-dependent alteration of doxorubicin pharmacokinetics by paclitaxel in a phase I study of paclitaxel and doxorubicin in patients with metastatic breast cancer, J. Clin. Oncol. 14 (1996) 2713–2721.
[53] J. Dong, J.I. Zink, Taking the temperature of the interiors of magnetically heated nanoparticles, ACS Nano 8 (2014) 5199–5207.
[54] T.P. Gustafson, Q. Cao, S.T. Wang, M.Y. Berezin, Design of irreversible optical nanothermometers for thermal ablations, Chem. Commun. 49 (2013) 680–682.
[55] M. Borzenkov, G. Chirico, L. D'Alfonso, L. Sironi, M. Collini, E. Cabrini, et al., Thermal and chemical stability of thiol bonding on gold nanostars, Langmuir 31 (2015) 8081–8091.
[56] Z. Zhang, L. Mei, S.-S. Feng, Paclitaxel drug delivery systems, Expet Opin. Drug Deliv. 10 (2013) 325–340.
[57] S.K. Sriraman, J. Pan, C. Sarisozen, E. Luther, V. Torchilin, Enhanced cytotoxicity of folic acid-targeted liposomes Co-Loaded with C6 ceramide and doxorubicin: in vitro evaluation on hela, a2780-adr, and H69-Ar cells, Mol. Pharm. 13 (2016) 428–437.
[58] H.S. Kim, Y.S. Lee, D.K. Kim, Doxorubicin exerts cytotoxic effects through cell cycle arrest and fas-mediated cell death, Pharmacology 84 (2009) 300–309.